Orientation of bluff body for designing efficient energy harvesters from vortex-induced vibrations

Dai, Hu Liang; Yang, Yaowen; Abdelkefi, A.; Wang, L.

2016

Dai, H. L., Abdelkefi, A., Yang, Y., & Wang, L. (2016). Orientation of bluff body for designing efficient energy harvesters from vortex-induced vibrations. Applied Physics Letters, 108(5), 053902-.

https://hdl.handle.net/10356/82444

https://doi.org/10.1063/1.4941546

Orientation of bluff body for designing efficient energy harvesters from vortex-induced vibrations

H. L. Dai, A. Abdelkefi, Y. Yang, and L. Wang

Citation: Applied Physics Letters **108**, 053902 (2016); doi: 10.1063/1.4941546
View online: http://dx.doi.org/10.1063/1.4941546
View Table of Contents: http://scitation.aip.org/content/aip/journal/apl/108/5?ver=pdfcov
Published by the AIP Publishing

Orientation of bluff body for designing efficient energy harvesters from vortex-induced vibrations

H. L. Dai,[1,2] A. Abdelkefi,[3] Y. Yang,[2,a)] and L. Wang[1]
[1]*Department of Mechanics, Huazhong University of Science and Technology, Wuhan 430074, China*
[2]*School of Civil and Environmental Engineering, Nanyang Technological University, Singapore 639798, Singapore*
[3]*Department of Mechanical and Aerospace Engineering, New Mexico State University, Las Cruces, New Mexico 88003, USA*

(Received 4 November 2015; accepted 27 January 2016; published online 4 February 2016)

The characteristics and performances of four distinct vortex-induced vibrations (VIVs) piezoelectric energy harvesters are experimentally investigated and compared. The difference between these VIV energy harvesters is the installation of the cylindrical bluff body at the tip of cantilever beam with different orientations (bottom, top, horizontal, and vertical). Experiments show that the synchronization regions of the bottom, top, and horizontal configurations are almost the same at low wind speeds (around 1.5 m/s). The vertical configuration has the highest wind speed for synchronization (around 3.5 m/s) with the largest harvested power, which is explained by its highest natural frequency and the smallest coupled damping. The results lead to the conclusion that to design efficient VIV energy harvesters, the bluff body should be aligned with the beam for low wind speeds (<2 m/s) and perpendicular to the beam at high wind speeds (>2 m/s). © *2016 AIP Publishing LLC*.
[http://dx.doi.org/10.1063/1.4941546]

Energy harvesting from flow-induced vibrations has been extensively studied in the past few years. Energy harvesters with efficient design are good candidates for powering small electronic devices[1–3] or replacing small batteries that have finite life span and require hard and expensive maintenance.[4–6] Flow-induced oscillations commonly utilized for energy harvesting include vortex-induced vibrations (VIVs),[7–10] transverse galloping,[11–13] wake galloping,[14] and flutter.[15–17] These mechanical vibrations can be converted into usable electrical power by piezoelectric and/or electromagnetic transduction, while the former has gained intensive attention due to its ease of application and high efficiency.

Important issues of aeroelastic energy harvesting include the optimal design of the harvester structure, the orientation and installation of the bluff body, and the effective energy extraction circuits. In this study, a particular focus is paid to investigate the influences of the orientation of the bluff body on the natural frequency, damping, synchronization region, and harvested power of VIV energy harvesters. Energy harvesting from VIV has received considerable attention due to its distinct properties, self-limited oscillations, and lock-in or synchronization region. The synchronization region takes place when the vortex shedding frequency is near the natural frequency of the cylindrical structure. Akaydin *et al.*[18] tested a piezoelectric energy harvester subjected to VIV in a wind tunnel. The effects of the resonant frequency and structural damping on the performance of the harvester were evaluated, and the optimal wind speed and peak harvested power were determined. Abdelkefi *et al.*[8] and Mehmood *et al.*[10] used a lumped-parameter model and studied the effects of the electrical load resistance on the synchronization region and levels of the harvested power. Dai *et al.*[19] developed and validated a nonlinear distributed-parameter model with the experimental measurements from Akaydin *et al.*[18] In addition, Dai *et al.*[20] investigated the impacts of the base excitations and vortex-induced vibrations on the performance of the harvester. Recently, Song *et al.*[21] investigated the VIV energy harvesting from water flows, showing that a lighter mass and a larger diameter of the attached cylinder can result in a better energy harvesting performance.

In these mentioned studies, characteristics of VIV-based piezoelectric energy harvesters were studied. However, no experimental study on various orientations of bluff body for VIV harvesters has been reported. In this letter, we design and test four distinct harvester configurations that consist of the same unimorph piezoelectric cantilever beam and a cylindrical bluff body. As shown in Fig. 1, various orientations/installations of the bluff body are considered in order to assess the impacts of gravity and aerodynamic force on the performance of the designed harvester. The bluff body of length 120 mm and diameter 30 mm is made of a light foam material. The active length, width, and thickness of the aluminum cantilever beam are 90 mm, 10 mm, and 0.6 mm, respectively. The total weight of the harvester is 5 g. A piezoelectric patch (MFC-M2807-P2, Smart Material Corp.) with a capacitance of 12.4 nF is bonded to the root of the beam and connected to an electrical load (R). The wind speed is measured by a Pitot tube anemometer, and the voltage across the load resistance is measured by the NI 9229 DAQ module.

The setup of four harvester configurations is shown in Fig. 1(b). The first three configurations (bottom, top, and horizontal) have the same installation, that is, the cylinder is attached to the beam end along its longitudinal direction, which is not usually adopted by other researchers. The cylinder is installed in different orientations to investigate the

a)Author to whom correspondence should be addressed. Electronic mail: cywyang@ntu.edu.sg

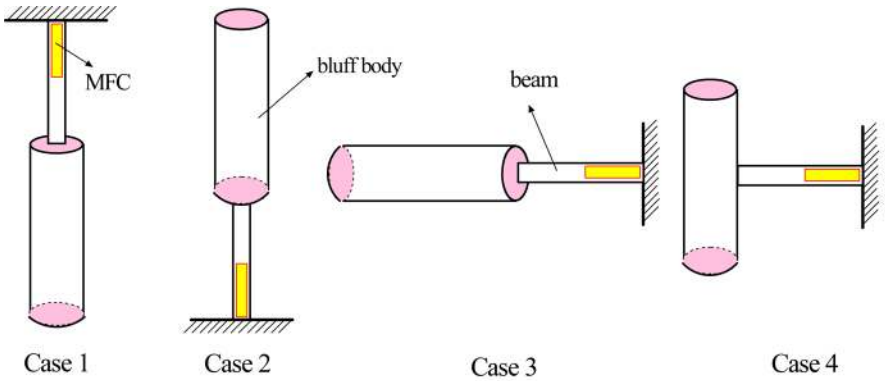

(a)

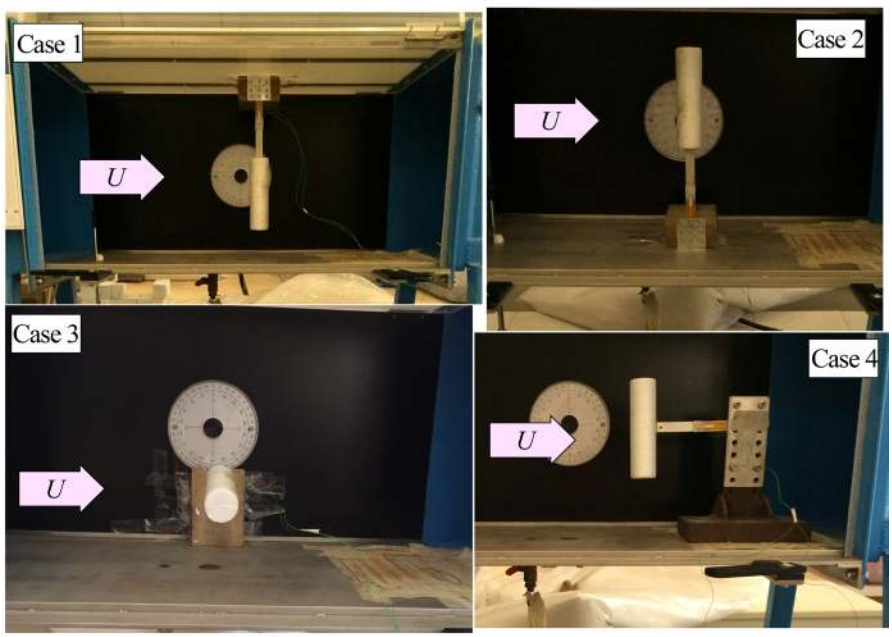

(b)

FIG. 1. (a) Schematic and (b) experimental setup of VIV-based energy harvester with different configurations (Case 1: bottom, Case 2: top, Case 3: horizontal, and Case 4: vertical).

effects of gravity and induced aerodynamic moment on the synchronization region and output performance of the harvester. As for the fourth configuration (Case 4: vertical), the cylinder is vertically aligned and perpendicular to the beam. This configuration has been used in previous studies,[12,18,20] which is also known by the negligible effect of the gravity and aerodynamic moment.

A lumped-parameter model for the VIV-based energy harvesters could be employed to explain their coupling behaviors, the governing equations are written as[8,10,12]

$$M_{eff}\ddot{w} + C\dot{w} + Kw + \Theta V = F_L, \tag{1}$$

$$C_p\dot{V} + \frac{V}{R} - \Theta\dot{w} = 0, \tag{2}$$

where w is the displacement of cylinder in the direction normal to the wind flow (U); M_{eff}, C, and K are, respectively, the effective mass, damping coefficient, and stiffness of the harvester, which are of difference for the four harvester configurations due to their distinct installations and orientations. Θ, C_p, and V are the electromechanical coupling coefficient, the capacitance of the piezoelectric sheet, and the generated voltage, respectively. F_L is the vortex-induced force, which can be empirically established based on the wake oscillator model.[19]

A free vibration test is conducted to obtain the open circuit ($R \approx \infty$) natural frequency and damping ratio for the four considered configurations. An initial displacement is given to the tip of the beam and the beam vibrates freely with the release of the initial displacement. During the free vibration, the time history of the voltage generated from MFC is recorded and plotted in Fig. 2. It is clear that for all configurations, the measured voltage gradually decays with time. For the same period of time, higher number of periods of oscillations (around 12 periods) is present in Case 4 as compared to the other three cases (around 6 periods). Case 4 thus has the largest natural frequency. Moreover, the amplitude of oscillations for Case 4 decreases at the lowest rate. In addition, the oscillations for Case 3 decay at a faster rate as compared to Cases 1 and 2. These observations are confirmed with the results in Table I, which are obtained by the Fast Fourier Transform (FFT) and log decrement techniques. In fact, the natural frequency for Case 4 almost doubles those for the other three cases. This is expected because the effective mass of the system increases when the aerodynamic moment is present in Cases 1 to 3, resulting in lower frequencies. In

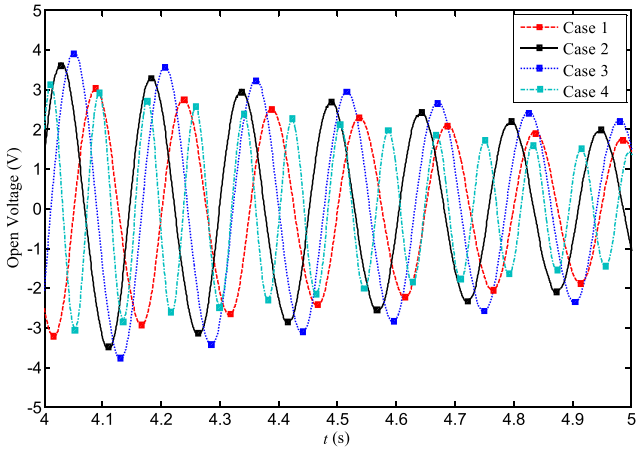

FIG. 2. Time history of generated voltage for four configurations under free vibration conditions.

addition, the damping ratio for Case 4 is the lowest, indicating the slowest decay in its oscillation amplitude.

It follows from Table I that the first three cases have natural frequencies between 6 Hz and 7 Hz as the harvesters have similar bluff body installation with the presence of the aerodynamic moment. It should be noted that the Case 1 (bottom) has a higher natural frequency as compared to Cases 2 and 3. This can be explained by the impact of gravity which produces a tension effect and hence an increase in the total stiffness of the system. Table I also shows that the placement of the cylinder plays an important role on the damping ratio. Case 3 (horizontal) has the highest damping ratio in comparison with Cases 1 and 2 (bottom and top). This may be due to the presence of the gravity effect in Cases 1 and 2. These free vibrations results are helpful to explain the discrepancies in the performances of different harvesters and their synchronization regions.

The plotted curves in Figs. 3 and 4, respectively, depict the variations of the root mean square (RMS) voltage and average power as functions of the wind speed for different load resistances, namely, $R = 10^4\ \Omega$, $10^5\ \Omega$, $10^6\ \Omega$, and $10^7\ \Omega$. The average harvested power is obtained by $P_{avg} = {V_{rms}}^2/R$, where V_{rms} is the root mean square voltage. It is observed in Figs. 3 and 4 that the synchronization region strongly depends on the installation/orientation of the cylinder. In fact, the synchronization region for the four configurations locates from 1.2 to 1.8 m/s, 1.1 to 1.9 m/s, 1.1 to 1.7 m/s, and 2.2 to 4.3 m/s, respectively. The maximum values of the generated voltage and power for the four cases take place when the wind speed is around 1.6 m/s, 1.6 m/s, 1.5 m/s, and 3.6 m/s, respectively. This dependency of the synchronization region and its resonant wind speed on the installation/orientation of the bluff body can be attributed to the associated change in the natural frequency, as presented in Table I. Since the natural frequency for Case 4 almost doubles those for the others, the resonant wind speed has a similar tendency. This is obvious from the direct relation between the wind speed (U) and the shedding frequency (ω_s) through the Strouhal number ($\omega_s = 2\pi S_t U/D$, where S_t is Strouhal number and D is diameter of the cylinder). It should be mentioned that a wide synchronization region is obtained in the vertical configuration (Case 4), which is very beneficial for efficient energy harvesting from VIV-based harvesters.

TABLE I. Natural frequencies and damping ratios of four configurations.

Case \ Characteristic	Natural frequency (Hz)	Damping ratio
1	6.8	0.0139
2	6.6	0.0135
3	6.4	0.0152
4	12.2	0.0109

Similar to the synchronization region, the harvested power is also significantly affected by the installation/orientation of the cylinder. Clearly, the generated voltage and power are the highest for Case 4, which is expected due to its lowest damping ratio and hence largest strain at the root of the cantilever. Case 3 has the lowest output voltage and power due to its high damping ratio (Table I).

From Figs. 3 to 4, we note that the load resistance has a negligible impact on the synchronization region, but it does have significant influence on the generated voltage and harvested power. It is clear that an increase in the electrical load is accompanied by an increase in the generated voltage for all cases, as shown in Fig. 3. On the other hand, the variation of the harvested power as a function of the load resistance is not monotonic, as shown in Fig. 4. It is noted that, when $R = 10^6\ \Omega$, the energy harvester can generate the highest power for all four configurations. This indicates the existence of an optimal load resistance at which the harvester can generate the maximum power.

In order to determine the optimal load resistance for all cases, we plot in Fig. 5 the variations of the average harvested power as a function of the load resistance at different wind speeds. Since Cases 1 to 3 (bottom, top, and horizontal) have the similar resonant wind speeds, the relationship between the harvested power and load resistance is presented in Fig. 5(a). For Case 1, the optimal load resistance does not depend on the wind speed, which is almost constant around 800 kΩ. For Case 2, the optimal load resistance varies between 500 kΩ (when $U = 1.6$ m/s) and 800 kΩ (when $U = 1.4$ and 1.5 m/s). For Case 3, it changes between 800 kΩ (when $U = 1.4$ and 1.6 m/s) and 1 MΩ (when $U = 1.5$ m/s). These small changes in the optimal load resistance for Case 1 to 3 are probably due to the differences in the natural frequency and damping ratio. For Case 4, the optimal load resistance is near 500 kΩ at all wind speeds, as presented in Fig. 5(b). We can conclude that the installation of the bluff body affects the synchronization region, the output voltage and power, and the optimal load resistance of the harvester. Consequently, depending on the placement of the harvester, a compromise between the installation/orientation of the bluff body and the load resistance should be considered.

A comparison of harvested power for all four cases when considering the optimal load resistance is presented in Fig. 6. The load resistance is set as 800 kΩ for Cases 1 to 3 and 500 kΩ for Case 4. For Cases 1 to 3, the lock-in region of the harvester is mainly between 1.2 m/s and 1.8 m/s due to their similar natural frequencies. However, small differences still exist in the harvested power and the bandwidth of the lock-in region. Clearly, Case 2 has a higher level of power as

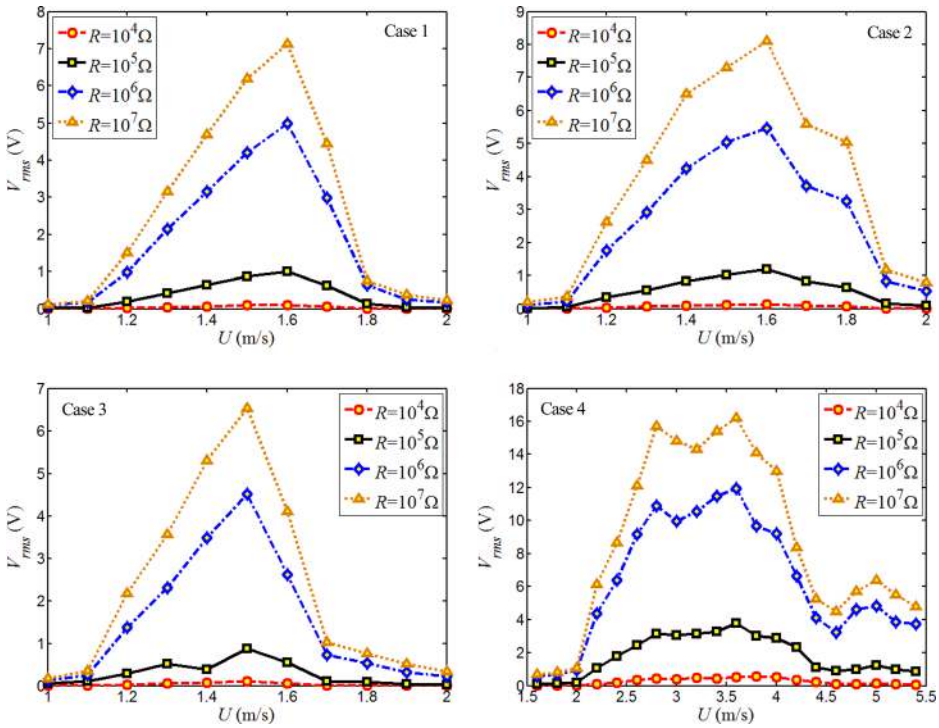

FIG. 3. Variations of generated voltage for four harvester configurations with wind speed for different electrical load resistances.

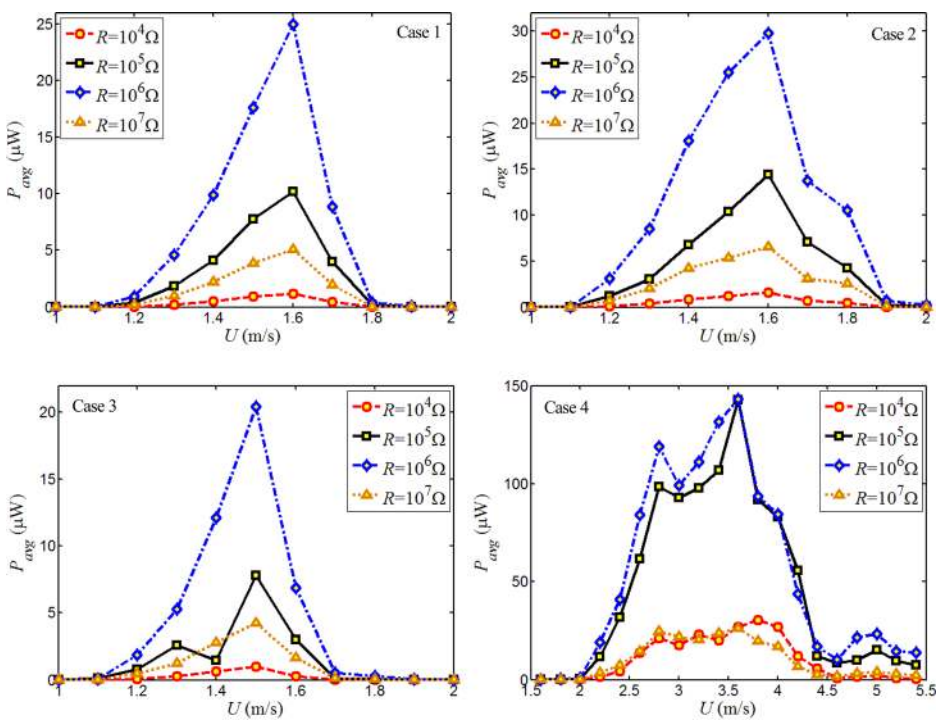

FIG. 4. Variations of generated average power for four harvester configurations with wind speed for different electrical load resistances.

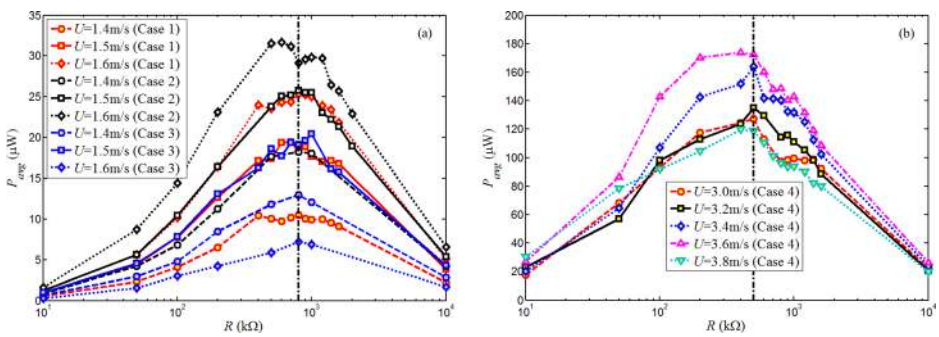

FIG. 5. Variations of average harvested power as a function of electrical load resistance for four configurations.

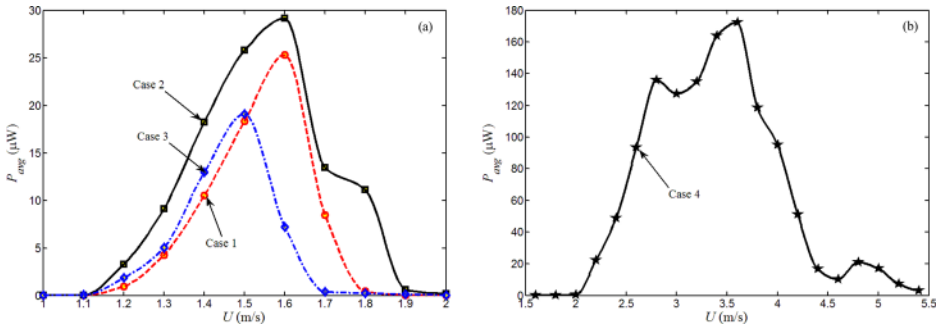

FIG. 6. Variations of average harvested power as a function of wind speed for different configurations: (a) Cases (1–3) when $R = 800\,\text{k}\Omega$ and (b) case 4 when $R = 500\,\text{k}\Omega$.

compared to Cases 1 and 3 because the damping ratio for Case 2 is lower. Case 3 has the lowest efficiency because of its highest damping ratio. Moreover, Case 3 possesses the narrowest synchronization region, which is not desired for efficient energy harvesting, as shown in Figure 6(a). Fig. 6(b) shows that for Case 4, the synchronization region is located between 2.2 and 4.4 m/s and the harvested power is significantly increased as compared to the other three cases. These can be explained by the highest natural frequency and lowest damping ratio for Case 4.

The performed analysis in this letter is helpful for the design of efficient VIV-based piezoelectric energy harvesters. It is demonstrated that, for small wind speeds between 1.3 and 1.8 m/s, the top configuration (Case 2) is the best candidate. For higher wind speeds between 3 and 4.4 m/s, the vertical configuration (Case 4) should be utilized. If the wind speed is increased (e.g., 10 to 20 m/s), the VIV energy harvesters should be re-designed to increase the shedding frequency and the natural frequency of these harvesters, which is necessary to fulfill the resonance condition in the lock-in region. To this end, a reduced tip mass could be a convenient solution, which would lead to an increase natural frequency of the VIV energy harvesters. The results and effects from the present study would still be valid for large wind speeds because the analysis is based on the characteristic of VIV. For example, if the first three VIV energy harvester configurations have their lock-in regions around 10 m/s, then, the fourth will have it larger than 10 m/s.

[1]S. P. Beeby, M. J. Tudor, and N. M. White, Meas. Sci. Technol. **17**, 175–195 (2006).
[2]A. Karami and D. J. Inman, Appl. Phys. Lett. **100**, 042901 (2012).
[3]N. Sharpes, A. Abdelkefiand, and S. Priya, Appl. Phys. Lett. **107**, 093901 (2015).
[4]H. Sodano, G. Park, and D. J. Inman, Shock Vib. Dig. **36**, 197–205 (2004).
[5]S. Roundy and P. K. Wright, Smart Mater. Struct. **13**, 1131 (2005).
[6]S. Priya, D. Popa, and F. Lewis, in Proceedings of ASME International Mechanical Engineering Congress and Exposition, Chicago, IL, 5–10 November 2006.
[7]H. D. Akaydin, N. Elvin, and Y. Andreopoulos, Exp. Fluids **49**, 291–304 (2010).
[8]A. Abdelkefi, M. R. Hajj, and A. H. Nayfeh, Nonlinear Dyn. **70**, 1377–1388 (2012).
[9]A. W. Mackowski and C. H. K. Williamson, Phys. Fluids **25**, 087101 (2013).
[10]A. Mehmood, A. Abdelkefi, M. R. Hajj, A. H. Nayfeh, I. Akhtar, and A. O. Nuhait, J. Sound Vib. **332**, 4656–4667 (2013).
[11]U. Javed, H. L. Dai, and A. Abdelkefi, Euro. Phys. J. Spec. Top. **224**, 2929–2948 (2015).
[12]Y. Yang, L. Zhao, and L. Tang, Appl. Phys. Lett. **102**, 064105 (2013).
[13]A. Bibo, A. Abdelkefi, and M. F. Daqaq, J. Vib. Acoust. **137**, 031017 (2015).
[14]A. Abdelkefi, J. M. Scanlon, E. McDowell, and M. R. Hajj, Appl. Phys. Lett. **103**, 033903 (2013).
[15]A. Erturk, W. G. R. Vieira, C. De Marqui, and D. J. Inman, Appl. Phys. Lett. **96**, 184103 (2010).
[16]V. C. Sousa, M. Anicezio, C. De Marqui, and A. Erturk, Smart Mater. Struct. **20**, 094007 (2011).
[17]A. Abdelkefi and A. O. Nuhait, Smart Mater. Struct. **22**, 095029 (2013).
[18]H. D. Akaydin, N. Elvin, and Y. Andreopoulos, Smart Mater. Struct. **21**, 025007 (2012).
[19]H. L. Dai, A. Abdelkefi, and L. Wang, J. Intell. Mater. Syst. Struct. **25**, 1861–1874 (2014).
[20]H. L. Dai, A. Abdelkefi, and L. Wang, Nonlinear Dyn. **77**, 967–981 (2014).
[21]R. Song, X. Shan, F. Lv, and T. Xie, Ceram. Int. **41**, S768–S773 (2015).